25th ABCM International Congress of Mechanical Engineering
October 20-25, 2019, Uberlândia, MG, Brazil

COB-2019-1627
NONLINEAR DYNAMIC ANALYSIS OF TORSIONAL FRICTION-INDUCED VIBRATIONS ON SLENDER STRUCTURES

Ingrid Pires
Hans I. Weber
Pontifícia Universidade Católica do Rio de Janeiro, 225 Marquês de São Vicente Street, Gávea - Rio de Janeiro, RJ - Brazil
ingridpires@icloud.com
hans@puc-rio.br

Bruno C. Cayres
Centro Federal de Educação Tecnológica Celso Suckow da Fonseca, Mario Covas Avenue, Santana - Itaguaí, RJ - Brazil
bruno.cayes@cafet-rj.br

Abstract. *Torsional vibration is present in most drilling routines, eventually reaching the stick-slip phenomenon. This type of vibration results from the nonlinear interaction between drill bits and rocks. Despite the complexity of the bit-rock interaction, researches often treat the relationship between torque and bit velocity as dry friction in a slender system. This contribution utilizes data from a test rig, capable of reproducing the torsional behavior experienced by real systems. We model the rig as an actuated torsional pendulum for the numerical investigation. Using the mathematical model, we numerically investigate the influence of the nonlinear control parameters in the system dynamics, and perform a stability analysis to identify stable solutions of the system.*

Keywords: *torsional vibrations, stick-slip, stability analysis*

1. INTRODUCTION

Stick-slip is a friction-induced limit cycle. In drilling operations, stick-slip happens when friction causes a complete arrest of the drill bit (stick phase), while the top drive continues to rotate until the stored energy overcomes the friction torque and the bit is released to rotate (slip phase). It is characterized by bit speed high fluctuations (Cayres *et al.*, 2018). These torsional vibrations result from the nonlinear bit-rock interaction (Wiercigroch *et al.*, 2018).

This contribution utilizes data from a test rig designed to offer similar dynamic properties as a drill string with simple brake devices to introduce friction, disturbing the rotating motion. We model the apparatus as an actuated torsional pendulum for the numerical investigation. This work intends to analyze the torsional behavior of the experimental system to prevent stick-slip phenomenon. In addition to that, we identify periodic solution and equilibria zones and predict large torsional vibration amplitudes. These results may provide background to future field applications in drilling processes.

2. EXPERIMENTAL TEST RIG

2.1 Test Rig description

The experimental apparatus used in this analysis was designed and built at Pontifícia Universidade Católica do Rio de Janeiro to reproduce the torsional oscillations experienced by real drill strings. The rig was designed to isolate the torsional from lateral and axial modes of vibration (Cayres, 2013). Figure 1 presents a picture of the test rig, a horizontal apparatus composed of an ENGEL GNM5480-G6.1 DC motor, a planetary gearbox with a reduction ratio of 8:1 coupled to the DC-motor, two solid discs, D1 and D2, and two low-stiffness shafts, that transmits the rotation from the DC-motor to the discs.

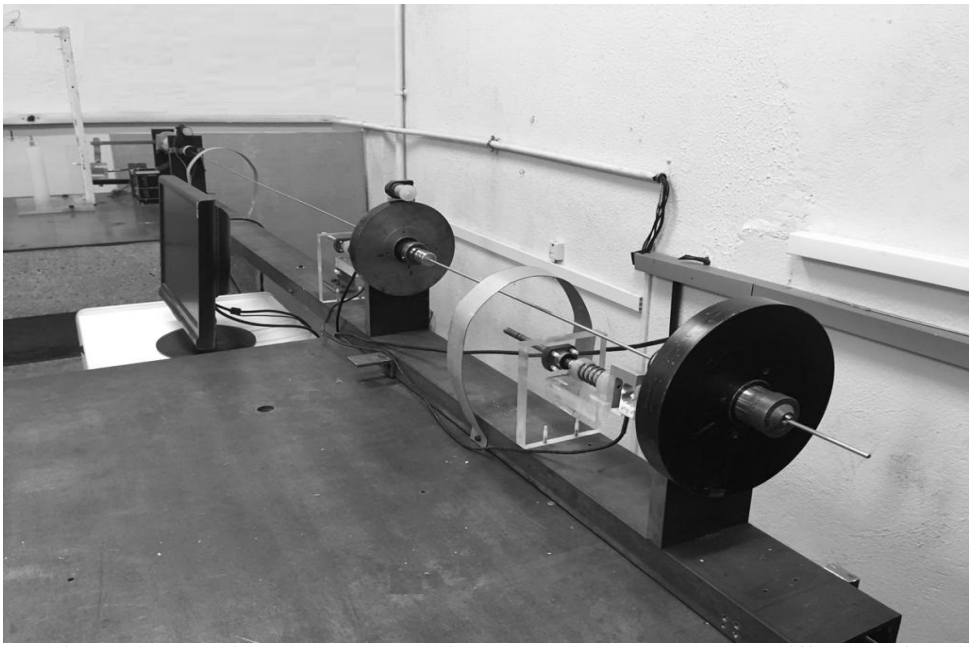

Figure 1: Experimental setup with DC-motor, two discs, D1 and D2, and two low-stiffness shafts (Pires, 2019).

There are two brake devices in the system to induce friction torque, placed in discs D1 and D2. The dry contact between the brake device pin and the disc produces friction torque, leading the system to experience torsional vibrations and stick-slip. The normal force produced by the pin and disc contact is acquired by load cells.

In this study, we are restricting our analysis to the reduced system composed of the DC-motor, the disc D2 and the shaft that connects them. Therefore, we are only considering the friction torque on the disc D2.

In addition to load cells, optical incremental encoders were placed on each disc and at the output of the motor planetary system to obtain all state variables of the system. The data is recorded by the National Instruments cDAQ system.

2.2 Test Rig modelling

This section introduces an experimental drill string setup dynamic model. Figure 2 presents a schematic system representation.

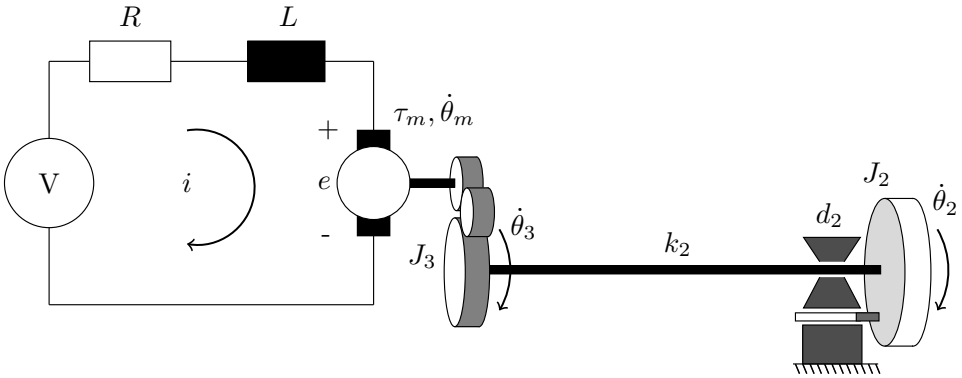

Figure 2: Schematic representation of the experimental setup with DC motor, two discs, and two shafts (Pires, 2019).

The mechanical subsystem is composed of disc D2, and the shaft connecting it to the DC-motor. Disc D2 has a moment of inertia J_2. The shaft torsional stiffness is denoted by k_2, and the linear damping is denoted by d_2. Although simple, torsional pendulum model can describe stick-slip phenomenon well. The electric subsystem is modeled as a voltage source connected in series with a resistor and an inductor. The mechanical and electrical systems coupling results in the following set of equations

$$\begin{aligned} J_2\ddot{\theta}_2 + d_2(\dot{\theta}_2 - \dot{\theta}_3) + k_2(\theta_2 - \theta_3) &= -T_{f2}, \\ d_2(\dot{\theta}_3 - \dot{\theta}_2) + k_2(\theta_3 - \theta_2) &= \eta(K_T i - C_m\eta\dot{\theta}_3 - T_f - J_m\eta\ddot{\theta}_3, \\ L\frac{di}{dt} + Ri + K_E\eta\dot{\theta}_3 &= V, \end{aligned} \tag{1}$$

where θ_2, $\dot{\theta}_2$, and $\ddot{\theta}_2$ are angular displacement, angular velocity and angular acceleration of D2, respectively, and T_{f2} is the resistive friction torque on disc D2. In Eq. (1), i denotes the DC-motor electric current, and L and R are the armature inductance and resistance, respectively. The angular velocity $\dot{\theta}_m$ is the velocity of the DC-motor inertia, J_m. C_m is the speed regulation; K_T, the constant motor torque; K_E, the voltage constant; and T_f, the internal friction torque. The input voltage is $V = \kappa_p(\omega_{ref} - \dot{\theta}_3) + \kappa_i \int_0^t (\omega_{ref} - \dot{\theta}_3)dt$,where κ_p and κ_i are proportional constant and integral constant, respectively, and ω_{ref} is the reference velocity of the system.

The resistive friction torque, T_{f2}, is mathmatically expressed as:

$$T_{f2} = \begin{cases} a\dot{\theta}_2 & \text{if } \left|\dot{\theta}_2\right| \leq \omega_s, \\ N_2 \cdot r \cdot (a1e^{(-((\alpha-b1)/c1)^2)} + a2e^{(-((\alpha-b2)/c2)^2)}) & \text{if } \left|\dot{\theta}_2\right| > \omega_s, \end{cases} \tag{2}$$

where $\omega_s = 10^{-3}$, r is the distance between the contact point and the rotation center of the disc D2, and N_2 is the normal contact force between pin and disc. The angle α is the torque friction position on the the phase space formed by the velocity and the acceleration of the disc D2 (Fig. 3), and the parameters a_i, b_i and c_i, $i = 1, 2$, are constants (Pires, 2019).

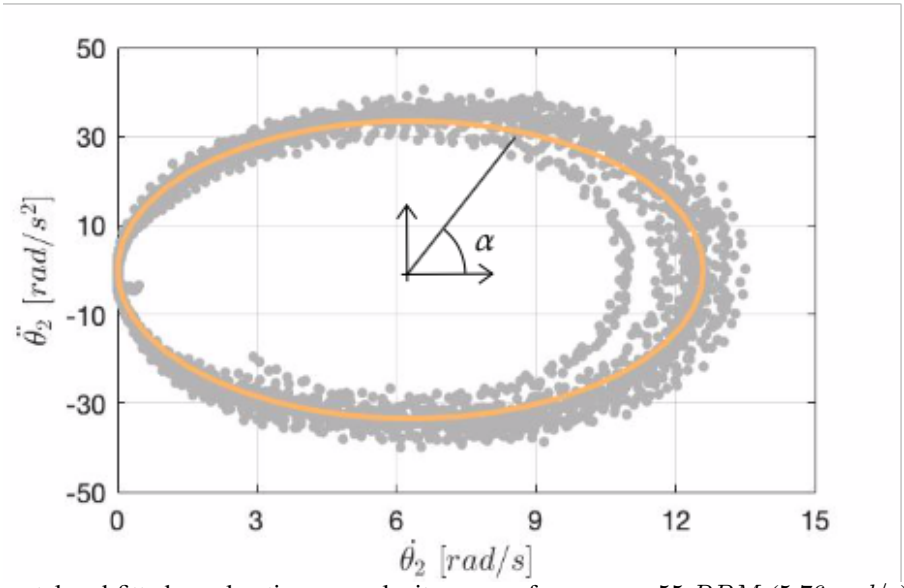

Figure 3: Experimental and fitted acceleration vs. velocity curves for $\omega_{ref} = 55\ RPM$ ($5.76\ rad/s$) and $N_2 = 50\ N$ (Pires, 2019).

3. EXPERIMENTAL RESULTS

This section investigates the experimentally observed torsional vibrations experienced by the reduced system, primarily the stick-slip phenomenon. This severe stage of torsional vibrations exists for different system conditions; in other words, different combinations of the control parameters (normal contact force and reference angular velocity). Moreover, the system exhibits different stick-slip responses depending on the control parameters combination.

To observe the influence of the reference angular velocity on the torsional vibrations of the rig, we varied ω_{ref} from 25 (2.62) to 55 (5.76) RPM (rad/s), in steps of 10 RPM (1.05 rad/s). Figure 4 presents the different rig torsional behaviors. Both Fig. 4(a) and Fig. 4(b) exhibit stick-slip phenomenon with different amplitudes, while Fig. 4(c) presents stick-slip with constant amplitude. At last, in Fig. 4(d), we can see torsional vibrations, but we do not observe stick-slip phenomenon. We acquired the system responses displayed in Fig. 4 for the same value of the normal contact force between the brake device and the disc D2, $N_2 = 10\ N$.

From Fig. 4 we can conclude that stick-slip phenomenon vanishes for high values of ω_{ref}. Moreover, one may notice that small values of ω_{ref} lead to more complex vibration time histories. In all cases of Fig. 4, we can observe the small oscillations in the speed of the motor inertia.

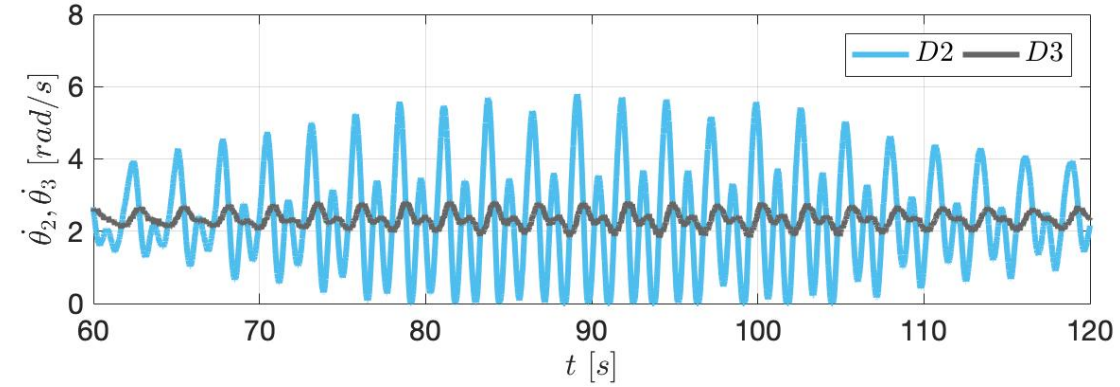

(a)

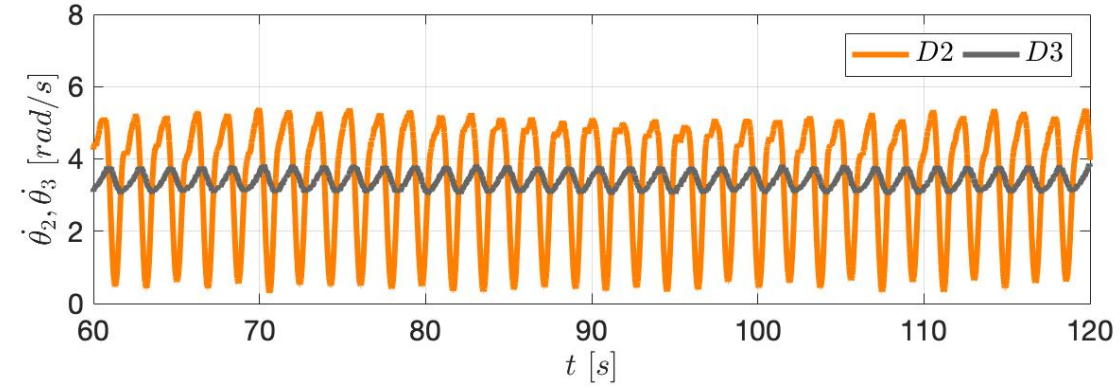

(b)

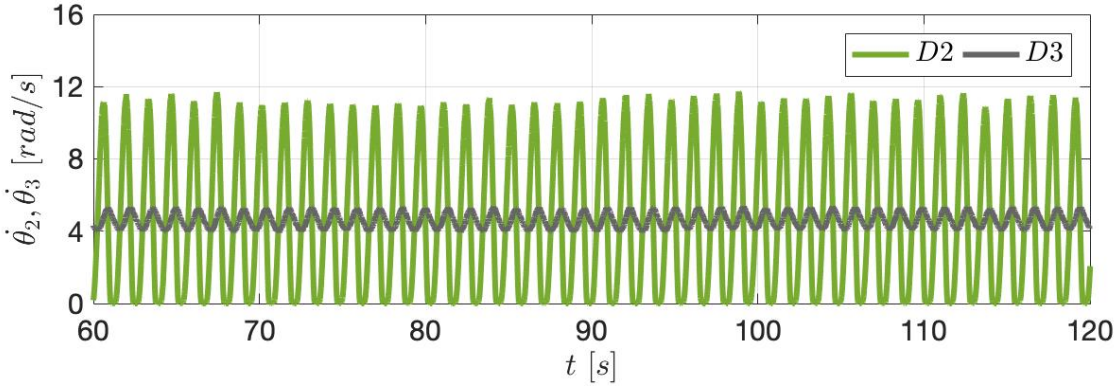

(c)

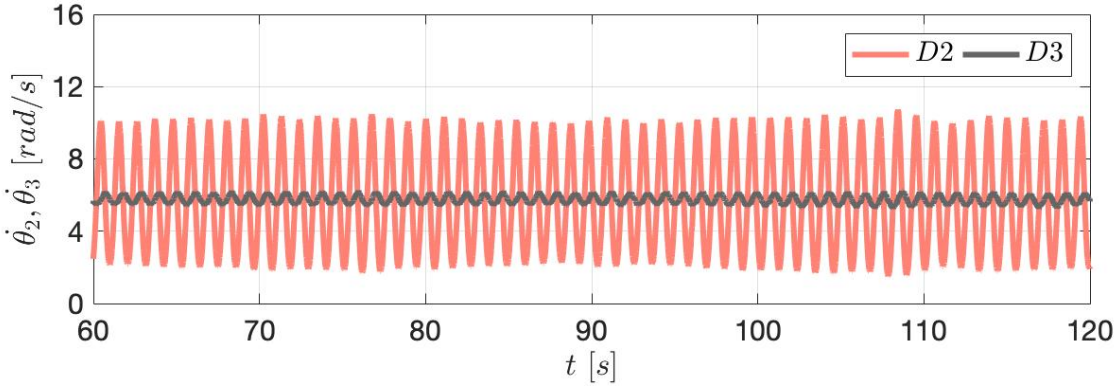

(d)

Figure 4: Torsional oscillations occurring in the reduced experimental rig for $N_2 = 10\ N$. The time histories of the angular velocities of D2 and D3 for (a) $\omega_{ref} = 25\ RPM$, (b) $\omega_{ref} = 35\ RPM$, (c) $\omega_{ref} = 45\ RPM$ and (d) $\omega_{ref} = 55\ RPM$ (Pires, 2019).

4. NONLINEAR ANALYSIS

4.1 Local stability

The qualitative structure of the dynamic behavior may change when specific parameters vary. It means that stable solutions can be created, destroyed, or become unstable (Strogatz, 2015). Then, the stability analysis is essential to identify changes in the system behavior when control parameters vary. As experimentally observed in the previous section, the system exhibits equilibrium and periodic solutions depending on the reference angular velocity, ω_{ref}. In the same way, the system may present different solutions depending on the value of the normal contact force, N_2.

Firstly, we perform an analysis of the basins of attraction for the same normal contact used in the previous section $N2 = 10\ N$. For this purpose, we use the torsional vibration factor, expressed as

$$f_{TV} = \frac{\mathtt{max}(\dot{\theta}_2) - \mathtt{min}(\dot{\theta}_2)}{2\,\omega_{ref}}, \tag{3}$$

For more information and discussion about this factor, see Cayres *et al.* (2018); Pereira *et al.* (2018).

Figure 5 presents the basins of attraction for different angular velocities ω_{ref}. The initial conditions were

$$x_0 = \begin{bmatrix} \delta_{23} & \dot{\theta}_2 & \dot{\theta}_3 & i \end{bmatrix}^T = \begin{bmatrix} \delta_{23} & \dot{\theta}_2 & \omega_{ref} & 1.04 \end{bmatrix}. \tag{4}$$

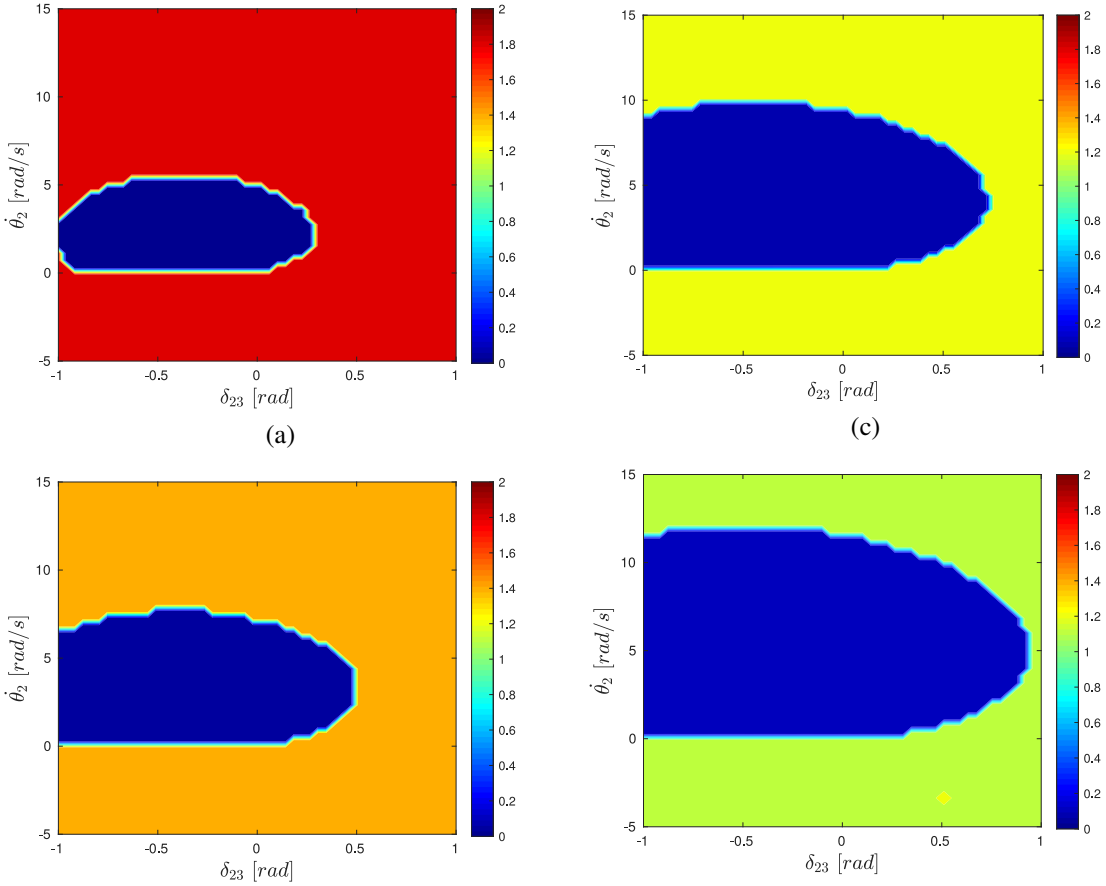

Figure 5: Basins of attraction of the reduced experimental rig for $N_2 = 10\ N$. (a) $\omega_{ref} = 25\ RPM$, (b) $\omega_{ref} = 35\ RPM$, (c) $\omega_{ref} = 45\ RPM$ and (d) $\omega_{ref} = 55\ RPM$.

Herein, we numerically obtained the electric current $i = 1.04\ A$, it represents the necessary current for the steady-state behavior (without torsional oscillations), and $\delta_{23} = \theta_2 - \theta_3$. One may observe that the equilibrium zone (the blue one) becomes bigger when $\omega_{ref} = 55\ RPM$, and the amplitudes of vibration become smaller. This is because of the DC-motor PI controller, responsible for regulating the angular velocity at D3, which introduces more energy into the system to overcome the friction torque.

4.2 Bifurcation diagrams

To observe the influence of the imposed velocity on the torsional vibrations, we varied it in the range from 0 to 60 (6.28) RPM (rad/s) for $N_2 = 10\ N$. Then we constructed a bifurcation diagram to identify the type of response for different ω_{ref}. Figure 6 presents the bifurcation diagram.

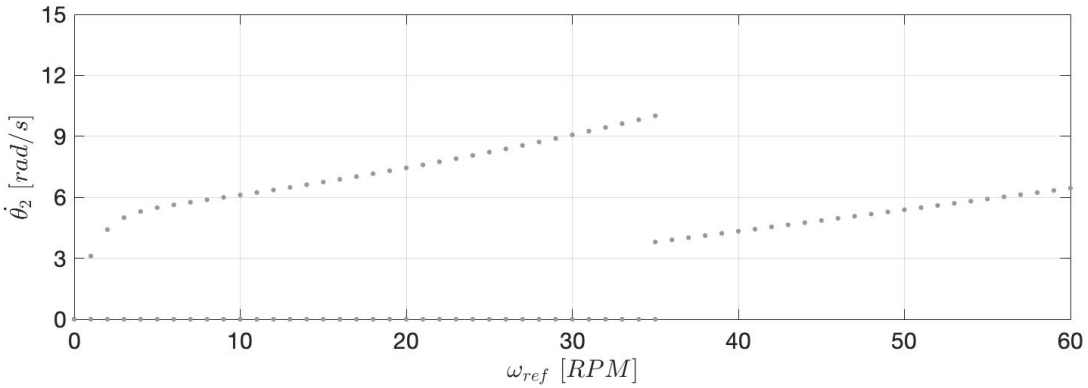

Figure 6: Bifurcation diagram with respect to reference angular velocity, ω_{ref}, for $N_2 = 10\ N$.

As ω_{ref} increases so do the amplitudes of stick-slip oscillations until it vanishes and we can only observe torsional oscillations. We expected this behavior because of experimental observations. In Fig. 4 one may notice that stick-slip phenomenon happens for values of ω_{ref} until $45\ RPM$. However, Fig. 6 presents a different value of ω_{ref} where the system response changes.

Similarly, we repeated the analysis to observe the influence of N_2 on the type of response. We varied it from 0 to 50 N for $\omega_{ref} = 55\ RPM$. The same parameters of torque friction curve are used for all of these cases, as $T_{f,2}$ depends on N_2 (Eq. 2). In the previous chapter, we observed that N_2 varies with the disc angle, although, for simplicity, in this analysis, we assume it to be constant. Figure 7 presents the bifurcation diagram with respect to N_2.

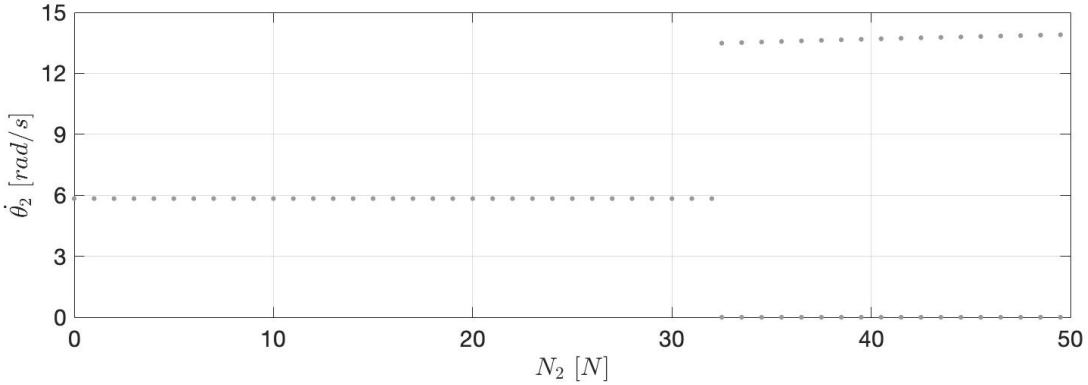

Figure 7: Bifurcation diagram with respect to normal contact force, N_2, for $\omega_{ref} = 55\ RPM$.

From Fig. 7, we notice that for the lower values of N_2 there are torsional oscillations. As N_2 increases so do the amplitudes of torsional oscillations, and stick-slip phenomenon appears.

5. FINAL DISCUSSIONS

This work has as its primary objective the analysis of the torsional behavior of an experimental test rig. This test rig offers torsional dynamic behavior similar to real drill strings. In this paper, we mathematically model the rig as an actuated torsional pendulum for numerical studies. Therefore, we study the influence of the control parameters on the type of response of the system, which includes the influences of both reference angular velocity and normal contact force - identifying periodic solutions and equilibria zones. From these analyses, we can conclude that the stick-slip phenomenon occurs in particular conditions. It is much more likely to appear for low values of reference velocity and high values of normal contact force.

6. ACKNOWLEDGEMENTS

The authors acknowledge the support given by CAPES.

7. REFERENCES

Awrejcewicz, J. and Olejnik, P., 2007. "Occurrence of stick-slip phenomenon". *Journal of Theoretical and Applied Mechanics*, Vol. Vol. 45 nr 1, pp. 33–40.

Cayres, B.C., 2013. *Numerical and experimental analysis of nonlinear torsional dynamics of a drilling system*. Master's thesis, Pontifícia Universidade Católica do Rio de Janeiro, Rio de Janeiro, Brasil.

Cayres, B.C., Fonseca, C., Sampaio, G. and Weber, H.I., 2018. "Analysis of a drill-string experimental set-up with dry friction-induced torsional vibration". In *Proceedings of the 10th International Conference on Rotordynamics - IFToMM*. Rio de Janeiro, Brazil.

Pereira, L.D., Cayres, B.C. and Weber, H.I., 2018. "Numerical application of a stick-slip control and experimental analysis using a test rig". In *MATEC Web of Conferences*. EDP Sciences, Vol. 148, p. 16009. doi: https://doi.org/10.1051/matecconf/201814816009.

Pires, I., 2019. *Torsional Friction-Induced Vibrations in Slender Rotating Structures*. Master's thesis, Pontifícia Universidade Católica do Rio de Janeiro, Rio de Janeiro, Brasil.

Strogatz, S.H., 2015. *Nonlinear Dynamics and Chaos*. Westview Press, Boulder, Colorado, 2nd edition.

Wiercigroch, M., Kapitaniak, M., Vaziri, V. and Nandakumar, K., 2018. "Complex dynamics of drill-strings: Theory and experiments". In *MATEC Web of Conferences, VETOMAC XIV*.